Natural Hazards (2021) 107:1981–2014
https://doi.org/10.1007/s11069-021-04673-1

ORIGINAL PAPER

GIS-based ensemble modelling of fuzzy system and bivariate statistics as a tool to improve the accuracy of landslide susceptibility mapping

Hassan Abedi Gheshlaghi[1,2] · **Bakhtiar Feizizadeh**[1,2]

Received: 13 October 2020 / Accepted: 28 February 2021 / Published online: 11 March 2021

Abstract
The primary objective is to propose and verify an ensemble approach based on fuzzy system and bivariate statistics for landslide susceptibility assessment (LSA) at Azarshahr Chay Basin (Iran). In this regard, various integrations of fuzzy membership value (FMV), frequency ratio (FR), and information value (IV) with index of entropy (IOE) were investigated. Aerial photograph interpretations and substantial field checking were used to identify the landslide locations. Out of 75 identified landslides, 52 (≈70%) locations were utilized for the training of the models, whereas the remaining 23 (≈30%) cases were employed for the validation of the models. Fourteen landslide conditioning factors including altitude, slope aspect, slope degree, lithology, distance to fault, curvature, land use, distance to river, topographic position index (TPI), topographic wetness index (TWI), stream power index (SPI), normalized difference vegetation index (NDVI), distance to road, and rainfall were prepared and utilized during the analysis. The FMV_IOE, FR_IOE, and IV_IOE models were designed utilizing the dataset for training. Finally, to validate as well as to compare the model's predictive abilities, the statistical measures of receiver operating characteristic (ROC), including sensitivity, accuracy, and specificity, were employed. The accuracy of 92.7, 92.5, and 91.8% of the models such as FMV_IOE, FR_IOE, and IV_IOE ensembles, respectively, was by the area under the receiver operating characteristic (AUROC) values developed from the ROC curve. For the validation dataset, the FMV_IOE model had the maximum sensitivity, accuracy, and specificity values of 95.7, 91.3, and 87.0%, respectively. Thus, the ensemble of FMV_IOE was introduced as a promising and premier approach that could be used for LSA in the study area. Also, IOE results indicated that altitude, lithology, and slope degree were main drivers of landslide occurrence. The results of the present research can be employed as a platform for appropriate basined management practices in order to plan the highly susceptible zones to landslide and hence minimize the expected losses.

✉ Hassan Abedi Gheshlaghi
hassanabedi3@yahoo.com

Bakhtiar Feizizadeh
Feizizadeh@tabrizu.ac.ir

[1] Department of Remote Sensing and GIS, University of Tabriz, Tabriz, Iran

[2] Institute of Environment, University of Tabriz, Tabriz, Iran

Keywords Landslide susceptibility · Conditioning factors · Ensemble approach · GIS

1 Introduction

Landslide is mass movements of soil or rock from the top to the bottom of a slope (Chen et al. 2018). It is known as one of the most significant and dangerous natural disasters worldwide, which leads to extensive social and economic losses along with the devastation of water and soil resources (Korup et al. 2012; Alimohammadlou et al. 2013; Raja et al. 2017). Thus, the occurrence of landslides is a complex phenomenon and is related to various parameters, i.e. geology, topography, vegetation, heavy rain, and activities of humans (Cruden 1991).

Worldwide from 1998 to 2017, landslides accounted 5.2% of natural hazards according to the information of the Centre for Research on the Epidemiology of Disasters (CRED 2018). Landslides caused global total annual damages of about 18 billion Euros (Zhu et al. 2018). Extensive sections of Iran are covered by mountainous regions, and therefore, landslide is commonly considered as natural disaster causing abundant economic and social losses (Shirzadi et al. 2017). Landslides happen in Iran mainly due to the Alpine–Himalayan belt activities (Farrokhnia et al. 2011; Shirzadi et al. 2017) which caused an economic loss of 10 billion USD with 4900 landslides occurrence till September 2007 (Shirani et al. 2018). Government agencies throughout the world have developed different approaches to alleviate and preclude the damages of landslides, including issuing early warnings, planning evacuation routes, and building engineering structures (Choi and Cheung 2013; Luo and Liu 2018). However, all of these techniques are dependent on the actual determination of spatial landslides prediction (Bui et al. 2016) which have properties that make them susceptible to land sliding, i.e. landslide susceptibility modelling (LSM) (Luo and Liu 2018).

The landslide susceptibility concept demonstrates the possibility of landslide events happening in an area based on the conditions of the local terrain, which do not include the return period nor the probability of happening of the instability process (Corominas et al. 2014; Zêzere et al. 2017). LSM is a solution for the apprehension and prediction of future landslides to alleviate their consequences (Feizizadeh and Blaschke 2013). Therefore, the generation of landslide susceptibility maps (LSMs) at the preliminary step of landslide hazard assessment is of significance for the safe economic planning. However, a standard procedure for the LSMs generation does not exist (Samodra et al. 2018).

It has been proven effective and feasible in recent decades to make use of geographic information system (GIS) and remote sensing (RS) technologies for the evaluation of landslide (Dou et al. 2019). A broad range of techniques and models have been suggested and employed for the LSM. The most usual approaches and procedures suggested in the literature are frequency ratio (Yilmaz 2009; Yalcin et al. 2011; Aditian et al. 2018), index of entropy (Constantin et al. 2011; Devkota et al. 2013; Youssef 2015), analytical hierarchy process (AHP) (Pourghasemi et al. 2012; Bahrami et al. 2020), analytical network process (ANP) (Melchiorre et al. 2008; Rajabi et al. 2016; Swetha and Gopinath 2020), information value (Du et al. 2017; Sharma and Mahajan 2019), fuzzy logic (Bui et al. 2012; Sahana and Sajjad 2017; Tsangaratos et al. 2018).

Comparatively the performance of these methods is good in LSM which can be improved further using hybrid methods to develop techniques (Bui et al. 2014; Truong et al. 2018). In recent years, researchers around the world have proposed various techniques, using hybrid and integrated approaches to generate LSM of distinct areas of the

world. These approaches include fuzzy logic and analytic hierarchy process (Gorsevski et al. 2006); fuzzy logic and ANP (Abedi Gheshlaghi and Feizizadeh 2017; Feizizadeh et al. 2021); AHP and statistical index (Arabameri et al. 2020); random forest base classifier and its ensembles (Ebrahimy et al. 2020; Nhu et al. 2020); fuzzy logic and weight of evidence (Hong et al. 2017); support vector machines and random subspace (Tien Bui et al. 2019); SVM and differential evolution (Tien Bui et al. 2016), and Bat algorithm optimized SVM (Bui et al. 2019).

The mentioned literature review reveals that world widely several techniques have been individually used. FMV, IV, and FR are such techniques which are capable to analyse the effect of factor classes on the occurrence of landslide. However, in most cases the correlation between the factors is neglected. On the contrary, the IOE is capable of analysing the association among the parameters, but it is not able to evaluate the factor classes. Therefore, there is a need of their integration into hybrid techniques for the landslide modelling. The above-cited hybrid models give rise to new thoughts of combining two distinct techniques in order to minimize the sensitivity to noises and isolated samples, thus appealing for many scholars (Meng et al. 2016). Combinations of index of entropy (IOE) with fuzzy membership value (FMV), information value (IV), and frequency ratio (FR) techniques can overcome the flaws of four approaches.

In this paper, new ensemble techniques, i.e. FMV_IOE, FR_IOE, and IV_IOE, have been proposed and substantiated for the LSM, with the case study of Azarshahr Chay Basin (ACB). Hence, the main purpose of this paper is to identify the landslide prone areas and to yield better predictions by developing the novel hybrid methods for LSMs. The major distinction between the present study and previous studies is that in this study three ensemble techniques are compared on the foundation of performance, and in the mapping of landslide susceptibility and for the first time their performance has been analysed. Fourteen factors were chosen as landslide controls factors: altitude, slope aspect, slope degree, lithology, distance to fault, curvature, land use, distance to river, topographic position index (TPI), topographic wetness index (TWI), stream power index (SPI), normalized difference vegetation index (NDVI), distance to road, and rainfall. They were created based on ArcGIS environment for the spatial analysis and manipulation of data. Finally, the LSMs were acquired and then compared with the three distinct integrated approaches. These maps provide important information for local landowners, planners to prepare emergency plans to minimize the negative effects on human life.

2 The study area and data used

2.1 The study area

The ACB is situated on the west side of the province East Azerbaijan with Urmia Lake spreading in its west side (Fig. 1). The lowest and highest elevation of the location under consideration is 1239 m a.s.l and 3300 m a.s.l, respectively (mean elevation 2282 m a.s.l.), with the slope variation from 0 to 75.95° (mean 11.06°).

The local climate can be separated into two different seasons, rainy and dry seasons. The dry season runs between June to September, while the rainy season runs between October and May. January is the coldest month with mean temperature of about −1 °C, and July is the hottest month of the region with mean temperature of about 27 °C. The geology of area is responsible for earthquakes, landslides, and volcanic hazards (Feizizadeh and Blaschke

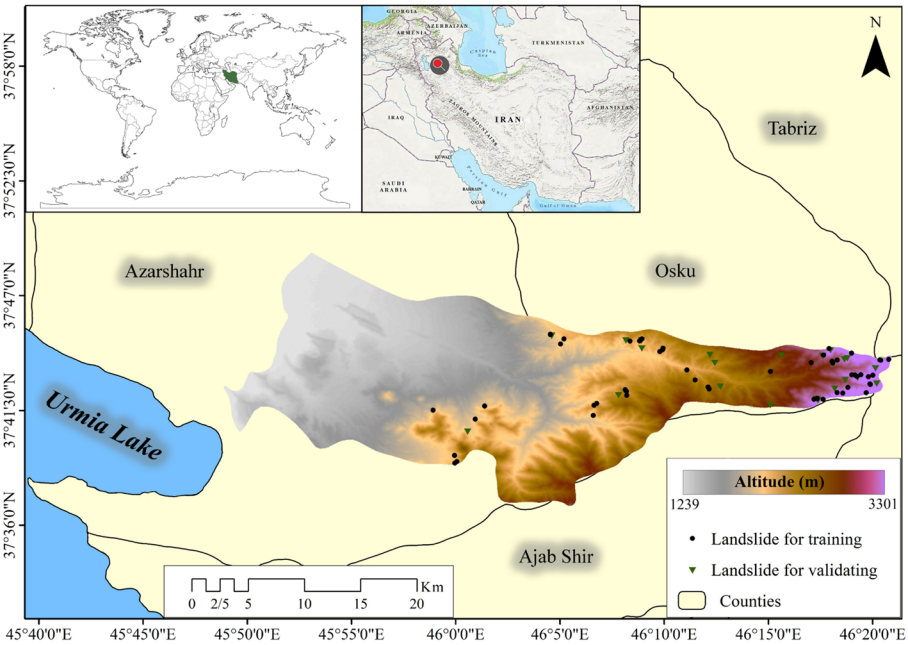

Fig. 1 Location of ACB

2013; Rahmati et al. 2019a, b). Various geologic units are included in the lithology of ACB such as dacitic andesite (35.14%) and yellow brecciated limestone and light-grey massive limestone (15.74%) (Table 1). The geological tectonic settings combined with unstable slopes make this area highly prone for hazards of landslide (Feizizadeh and Blaschke 2013). The land use includes agricultural land, orchard land, grassland, barren land, and

Table 1 The lithology of ACB

No.	Symbol or code	Description
1	Q^{sd}	Salt-clay deposits
3	PLQ^{ash}	Volcanic ashes with block, lahar and welded breccia (Pelean)
2	Ng^{ct}	Tuff breccia with intercalations of Conglomerate and sandstone
4	PLQ^{d}	Dacitic andesite
6	Q_2	Old terraces and alluvial fan deposits
5	Q^{tr}	Travertine
7	Ng^{b}	Volcanic breccia with pyroxene andesite
8	Q_3	Young terraces and alluvial fan deposits, locally including cultivated
10	J_d	Light grey to whitish, thin to thick-bedded ammonite and belemnite bearing argillaceous limestone (Dalichai Formation)
9	J_l	Limestone and dolomitic limestone
13	K^{c}_{l}	Red conglomerate, sandstone and siltstone
12	JK_l	Yellow brecciated limestone and light-grey massive limestone (Lar Formation)
11	K^{l}_{l}	Grey to dark grey, Orbitolina bearing, argillaceous-limestone and limestone

cultivation and built-up area, whereas maximum area is covered by grassland (58.54%). In this area, massive rain and unfit practices of land use contribute to natural hazards, i.e. landslides, flooding, and erosion of soil during past several years.

Due to its steep slopes, absence of full-scope shelter by vegetation, unconsolidated soil and materials of surface and various active processes over the year, this region is one of the watersheds of the Sahand Mountains. It has been made as one of the areas prone to mass movements because of human's indirect manipulation in recent decades (Abedi Gheshlaghi and Feizizadeh 2017). In the study area, most of the landslides occur during rainy season. Mostly landslide events can be contemplated as a rotational landslide according to the observations (Feizizadeh and Blaschke 2013) and the statements of field observations.

2.2 Landslide inventory

Future risk events of a specific location may be estimated through the assessment of the records of past happenings (Devkota et al. 2013; Abedi Gheshlaghi 2019; Costache and Bui 2019; Rahmati et al. 2019a, b). The requisite input for examining the association between the spatial dissemination of landslides and the conditioning factors is the landslide inventory map (Chen et al. 2019b). Therefore, in the assessment of landslide susceptibility, the primary step is the assessment of similar past happenings and their conditioning factors. In this research, a landslide inventory was acquired utilizing images of Google Earth employing Google Earth software and field surveys through GPS. The obtained landslide inventory included 75 landslide conditions, which were classified randomly into two classes, for training (≈70%) and validation (≈30%). This inventory of landslide consists of translational (20 points), rotational (43 points), and debris flows (12 points). Landslide destruction example in the study region is depicted in Fig. 1.

2.3 Landslide conditioning factors

An essential step in LSM is the proper selection of conditioning factors for a landslide to find the spatial association between landslide inventory happenings and geo-environmental factors. In ACB, the conditioning factors were chosen after taking into account many existing studies related to landslide susceptibility as well as the field investigation (Gariano and Guzzetti 2016; Alvioli et al. 2018). Afterwards, the parameters of slope degree (Fig. 2a), slope aspect (Fig. 2b), altitude (Fig. 2c), lithology (Fig. 2d), land use (Fig. 2e), distance to river (Fig. 2f), distance to road (Fig. 2g), distance to fault (Fig. 2h), NDVI (Fig. 2i), curvature (Fig. 2j), SPI (Fig. 2k), TPI (Fig. 2l), TWI (Fig. 2m), and rainfall (Fig. 2n) were utilized for the mapping of landslide susceptibility. Detailed information is available in Table 2 which includes sources of data, GIS data type, and related LSM factor classes.

For the preparation of slope, curvature, altitude, TWI and SPI factors in ArcGIS 10.6 environment, the digital elevation model (DEM) of the county having a spatial resolution of 30 m was acquired from the United States Geological Survey (USGS, http://www.usgs.gov).

In our study for checking the multicollinearity between the landslide conditioning factors, the tolerance (TOL) and variance inflation factor (VIF) were employed. These methods are mostly used for checking the multicollinearity between independent variables (Chen et al. 2018; Arabameri et al. 2019a), and critical multicollinearity between the conditioning factors is shown by a TOL value b of 0.1 or a VIF value N5 (Chen et al. 2018).

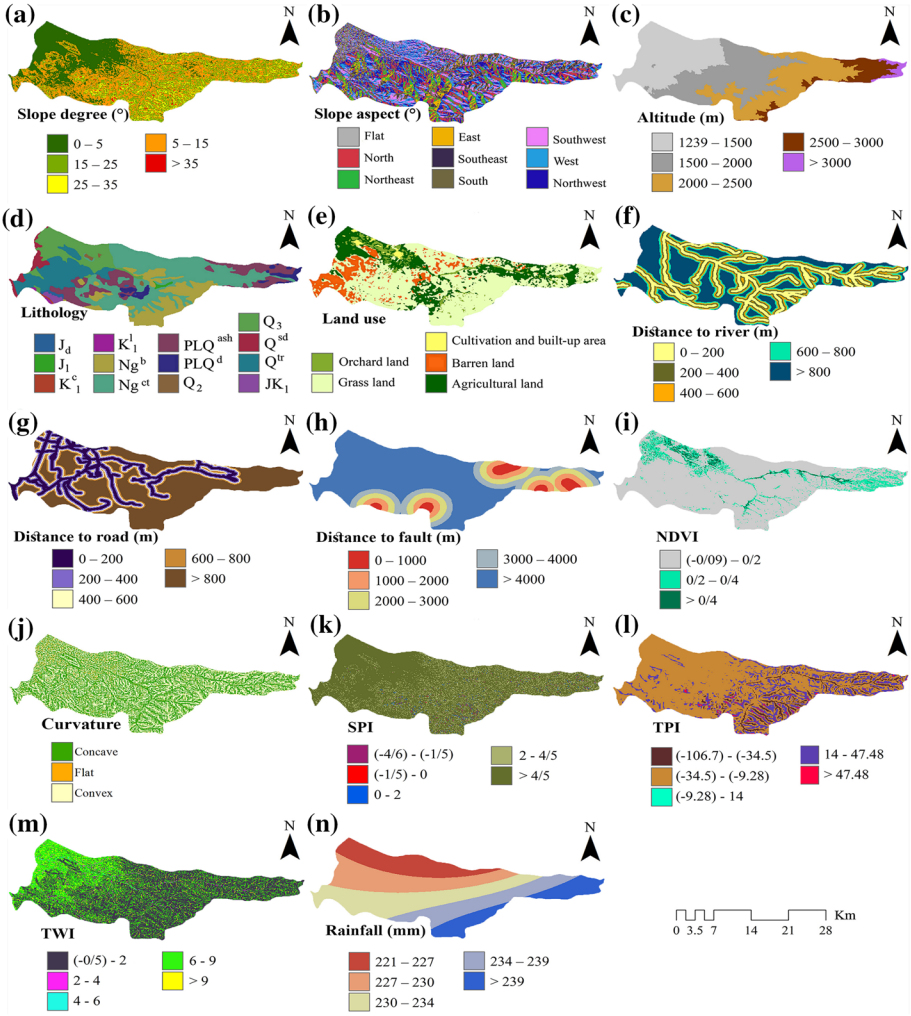

Fig. 2 Maps of thematic: **a** slope degree; **b** slope aspect; **c** altitude; **d** lithology; **e** land use; **f** distance to river; **g** distance to road; **h** distance to fault; **i** NDVI; **j** curvature; **k** SPI; **l** TPI; **m** TWI; **n** rainfall

2.3.1 Slope degree

According to the researchers, the most significant factor in landslide stability assessment is always the slope degree (Reichenbach et al. 2018) because it directly influences the shear forces (Lee and Min 2001). The slope degree classifications of the region under consideration were acquired from a DEM with 30 m spatial resolution. It was categorized into five classes, namely: 0–5°, 5–15°, 15°–25°, 25°–35°, and > 35° (Fig. 2a). The investigation of spatial distribution exhibits that about 42.31% of the landslides in the region under study were noticed on the slope degree of 15–25° (Fig. 3a).

Table 2 The source data for conditioning factors and landslide inventory

Sub-classification		Data source	GIS data type		Resolution or scale
Spatial dataset	Data parameter		Spatial dataset	Map of derived	Spatial dataset
Landslide inventory	Landslide inventory	Images of google earth	Point	–	–
		Field surveys through GPS			
Topographic map	Altitude	ASTER GDEM	GRID	Slope degree (°)	30 m
	Slope			Aspect (°)	
	Aspect			Altitude (m)	
	Curvature			Curvature (100/metre)	
	TPI			Topographic position index	
	SPI			Stream power index	
	TWI			Topographic wetness index	
River	Distance to river		ARC/INFO Line coverage	Distance to river (m)	
Road	Distance to road	Iran Ministry of Roads and Urban Development		Distance to road (m)	
Rainfall	Rainfall	Iran Meteorological Organization	GRID	Rainfall (mm)	
Geology Map	Lithology	Iran Geology Organization	ARC/INFO coverage	Lithology	1:100,000
	Distance to fault		ARC/INFO Line coverage	Distance to fault (m)	30 m
Normalized difference vegetation index	NDVI	Landsat-8 satellite images	ARC/INFO GRID	NDVI	
Land use type	Land use			Land use	

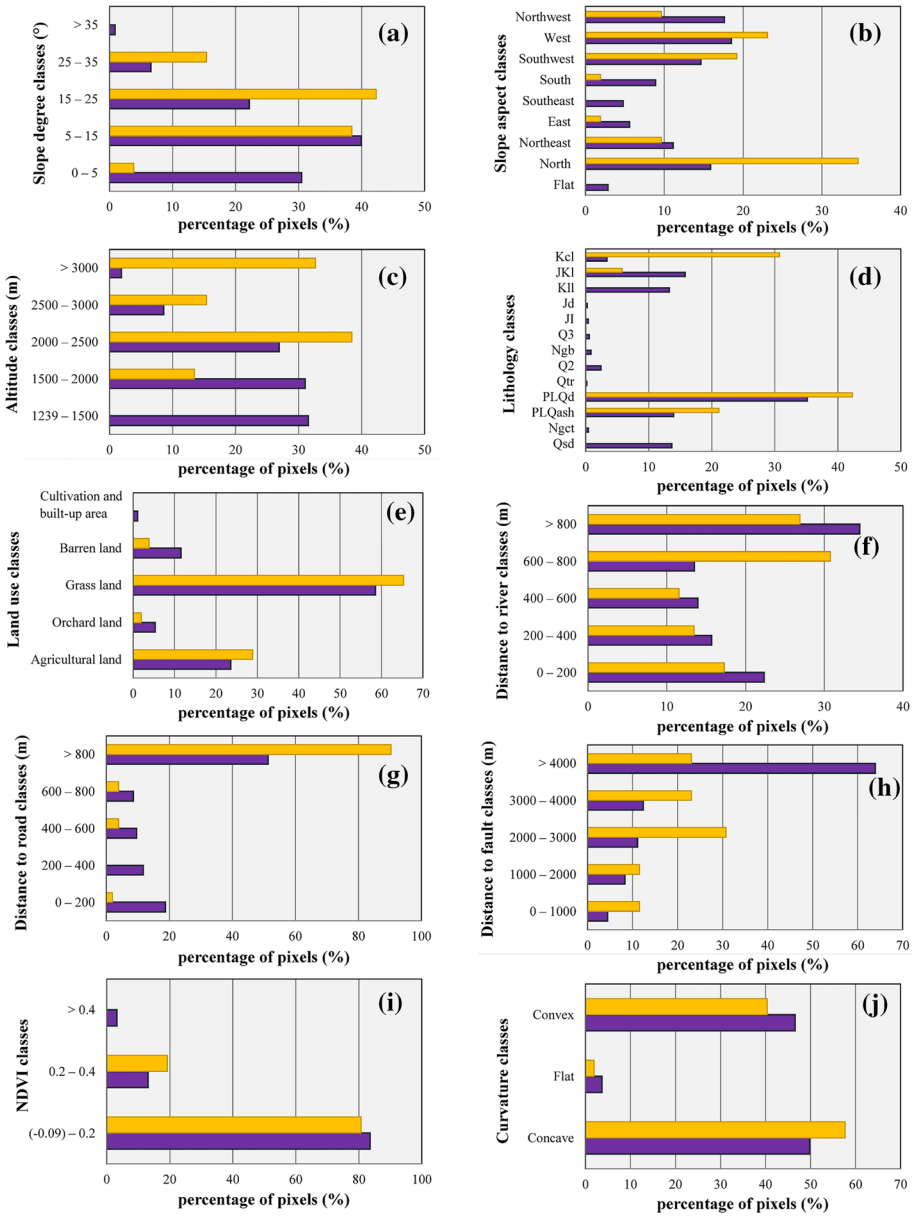

Fig. 3 Analysis of landslide conditioning factors: **a** slope degree; **b** slope aspect; **c** altitude; **d** lithology; **e** land use; **f** distance to river; **g** distance to road; **h** distance to fault; **i** NDVI; **j** curvature; **k** SPI; **l** TPI; **m** TWI; **n** rainfall

2.3.2 Slope aspect

The direction of the highest slope of the terrain surface is known as slope aspect (Meng et al. 2016) and is a crucial topographic factor that affects moisture on slopes due to

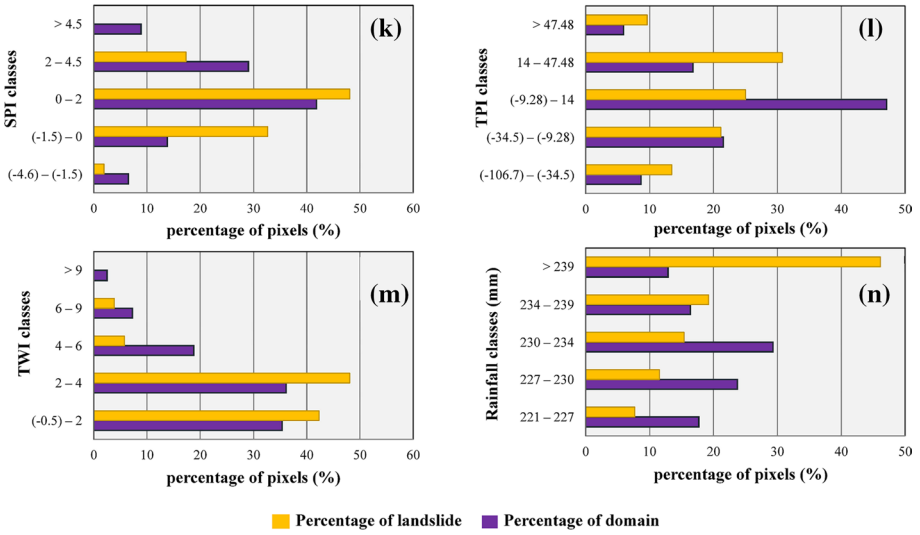

Fig. 3 (continued)

radiation from the sun and rainfall depending on the slope facing directions (McKean and Roering 2004; Pham et al. 2018). DEM was utilized for the acquisition of the slope aspect map. The map of the slope aspect was developed with nine intervals, including flat, east, north, northeast, southwest, south, southeast, west, and northwest (Fig. 2b). Slope aspect frequency assessment (Fig. 3b) manifests that the majority of landslide event happenings are in the north direction (34.62%), west (23.08%), and southwest (19.23%).

2.3.3 Altitude

Altitude which is the height above the sea level is familiar for its effects on biological as well as natural factors (Kavzoglu et al. 2014). Various geomorphological and geologic processes controlled this parameter (Ayalew and Yamagishi 2005). Altitude was categorized into five categories: 1239–1500, 1500–2000, 2000–2500, 2500–3000, and > 3000 m (Fig. 2c). Landslide frequency assessment exhibited that the majority of landslides were recorded in the group of 2000–2500 (38.46%) (Fig. 3c).

2.3.4 Lithology

One of the principals and basic factors having direct influence on the landslides occurrence is lithology (Abedini et al. 2018; Jiménez-Perálvarez 2018) since lithological and structural alterations usually lead to variations in durability and porosity of rocks as well as soils (Kavzoglu et al. 2014). Many researches have considered lithological features as impact factors for the susceptibility of landslide (Chen et al. 2016; Rosi et al. 2018; Dang et al. 2019). The map of lithology (Fig. 2d) was created by the Geological Survey of Iran at a scale of 1:100,000 (Table 1). Frequency evaluation of landslide happenings on lithology shows that majority of the landslides (42.31%) are located on dacitic andesite which occupies about 35.14% area (Fig. 3d).

2.3.5 Land use

Alterations in the environment and activities of humans affect land use (Kalantar et al. 2018). According to Pourghasemi et al. (Pourghasemi et al. 2018), it is the maximum utilized predictor layer after lithology, slope, and aspect which can be generated using techniques of remote sensing (Guan et al. 2017; Pham et al. 2018; Yang et al. 2019). For this research, map of land use was generated from OLI of Landsat 8 images in connection with the field maps. Land use in the region under consideration is categorized into five categories: agricultural land, orchard land, grassland, barren land, and cultivation and built-up area (Fig. 2e). Frequency assessment on land use (Fig. 3e) data of the region under study suggests that the majority of landslides are observed in grassland area (65.38%).

2.3.6 Distance to river

In the stability of the landslide, the distance to the rivers conditioning parameter plays an effective role (Dehnavi et al. 2015; Abedini et al. 2018). The measure of distance to river has been utilized in numerous studies as an impact factor (Nicu and Asăndulesei 2018; Moayedi et al. 2019). The river network was generated from DEM and grouped into five buffer groups: 0–200, 200–400, 400–600, 600–800, and > 800 m (Fig. 2f). The results of the analysis show that about 30.77% landslides are distributed from 600–800 m distance in river valley (Fig. 3f).

2.3.7 Distance to road

Distance to road has a significant association with the landslide event happening that can be the result of cut slope formations through the building of roads which disturbs the natural topology and impacts the slope stability (Kavzoglu et al. 2014). Distance to road is often utilized in the assessment of landslide susceptibility in numerous studies and is known as one of the causal parameters for the landslide event (Chen et al. 2019a). In the current research, distance to roads was considered for the landslide susceptibility and grouped into five zones of buffer making use of 200 m interval (Fig. 2g): 0–200, 200–400, 400–600, 600–800, and > 800 m. The output of the frequency assessment (Fig. 3g) manifests that high number of landslides are observed in > 800 mm (62.67%).

2.3.8 Distance to fault

Faults form a zone or line of weakness specified by tectonic structure (Meng et al. 2016). The distance to faults is an important parameter in the mapping of LSM (Abedini et al. 2018). Proximity to these structures escalates the chances of the occurrence of landslides (Bourenane et al. 2016). In this research, the distance to faults was generated from the structural geology map of the area under study at a scale of 1:100,000 and was grouped into five groups using 1000 m interval based on the ArcGIS 10.6 software, and the fault buffer categories were specified as 0–1000, 1000–2000, 2000–3000, 3000–4000, and > 4000 m (Fig. 2h). Results indicate that the majority of the landslides are nearly

equally disseminated within these classes: 2000–3000 m (30.77%); 3000–4000 m (23.08%); and > 4000 m (23.08%) (Fig. 3h).

2.3.9 NDVI

The landslides occurrence is closely associated with the density of vegetation (Meng et al. 2016). The NDVI is a parameter that can detect an increase in vegetation and vegetation coverage (Hong et al. 2016). The map of NDVI for the present research was developed from the Landsat-8 satellite images associated with the OLI-sensor making use of the equation given below (Hong et al. 2016):

$$\mathrm{NDVI} = (\mathrm{NIR} - \mathrm{RED})/(\mathrm{NIR} + \mathrm{RED}) \tag{1}$$

where NIR is the near-infrared band (0.85–0.88 μm, Band 5) and RED is the red band (0.64–0.67 μm, Band 4). For the current research, the map of NDVI was created with three intervals, including (−0.09)–0.2, 0.2–0.4, and > 0.4 (Fig. 2i). Landslide frequency assessment manifests that maximum landslides were observed in the group of (−0.09)–0.2 (80.77%) (Fig. 3i).

2.3.10 Curvature

Curvature influences the events of landslide beside other geo-environmental, and topographic factors as the movement of water depends on the curvature of the ground surface (Pham et al. 2018). Positive value of curvature shows convexity, zero value exhibits the flat areas, and negative value manifests concavity (Fig. 2j). Landslides are nearly equally disseminated in concave (57.69%) and convex (40.38%) groups (Fig. 3j).

2.3.11 SPI, TWI, and TPI

The SPI, TPI, and TWI are three important hydrologic factors that can assess the spatial alteration of landslide-vulnerable areas. They are broadly utilized in the mapping of landslide susceptibility (Kalantar et al. 2018; Pourghasemi et al. 2018). The SPI represents the erosion strength of streams which might affect the occurrence of landslide (Raja et al. 2017). TWI commonly supplies a means of quantification of the topographical influence on the hydrological activities (Tehrany et al. 2019). Maximum TWI values were related to the wet regions, whereas the minimum values with dry regions (Laamrani et al. 2015). ArcGIS software was utilized to create SPI and TWI from DEM making use of the equations given below:

$$\mathrm{TWI} = \ln(A_s/\tan\beta) \tag{2}$$

$$\mathrm{SPI} = A_s \tan\beta \tag{3}$$

where A_s is the particular catchment region ($m^2\ m^{-1}$), and β (radian) is the slope gradient (in degrees). The maps of TWI and SPI of the watershed were developed with five intervals, including SPI: (−4.6)–(−1.5), (−1.5)–0, 0–2, 2–4.5, and > 4.5; TWI: (−0/5)–2, 2–4, 4–6, 6–9, and > 9 (Fig. 2k–m). The SPI density of 0–2 and in the case of TWI as 2–4 is highly vulnerable to the landslide occurrence (48.08%) (Fig. 3k–m).

TPI was computed in ArcGIS software by employing the equation given below:

$$TPI = E_c - \left(\frac{1}{n^M} \sum_{i \epsilon m} E_i \right) \tag{4}$$

where E_c is the elevation at the central point, E_i is the elevation and M is the predetermined radius (predetermined matrix length) (Kavzoglu et al. 2015). The watershed TPI map was developed with five intervals, including: (−106.7)–(−34.5), (−34.5)–(−9.28), (−9.28)–14, 14–47.48, and > 47.48 (Fig. 2l). Maximum landslides were observed in TPI of 14–47.48 (30.77%) (Fig. 3l).

2.3.12 Rainfall (mean annual)

The most influential factor for landslide occurrence is the high-intensity rainfall (Youssef 2015). The landslides induced by rainfall have been widely studied by scholars (Yano et al. 2019). The map of rainfall map was created making use of the inverse distance weighted (IDW) technique for the period 2005–2015 at the Tabriz, Sahand, Ajabshir, Bonab, and Maragheh stations and then grouped into five groups including 221–227, 227–230, 230–234, 234–239, and > 239 mm (Fig. 2n). The output of the frequency assessment (Fig. 3n) manifests that high number of landslides are observed in > 239 mm (46.15%).

3 Methodology

The susceptibility modelling was carried out employing the ensemble FMV_IOE, FR_IOE, and IV_IOE methods. The proposed methodology in the present study has been carried out in seven main phases: (a) preparation of the spatial database; (b) selection of the conditioning factors for landslide analysis; (c) preparation of training and validation datasets; (d) development of the hybrid landslide models; (e) generation of the LSMs; (f) validation and comparison of the three models; (g) selection of the best model. The procedures of selected techniques are stepwise shown in Fig. 4.

3.1 Frequency ratio (FR)

FR model can be utilized to quantify the spatial association between dependent and independent variables and is a bivariate statistical method (Termeh et al. 2018). The spatial association between landslides and conditioning factors was employed in the FR technique. It was computed by employing the equation given below:

$$\mathrm{FR} = \frac{A_i / A}{B_i / B} \tag{5}$$

where A_i is the landslide pixels number within each group area, A represents the number of total landslides in the region under study, B_i exhibits the number of the pixels in the conditioning factor group, and B is the number of total pixels in the region under consideration. If the weights are less than 1, then it represents a minor correlation, whereas if they are more than 1, then it represents a higher correlation (Lee and Min 2001).

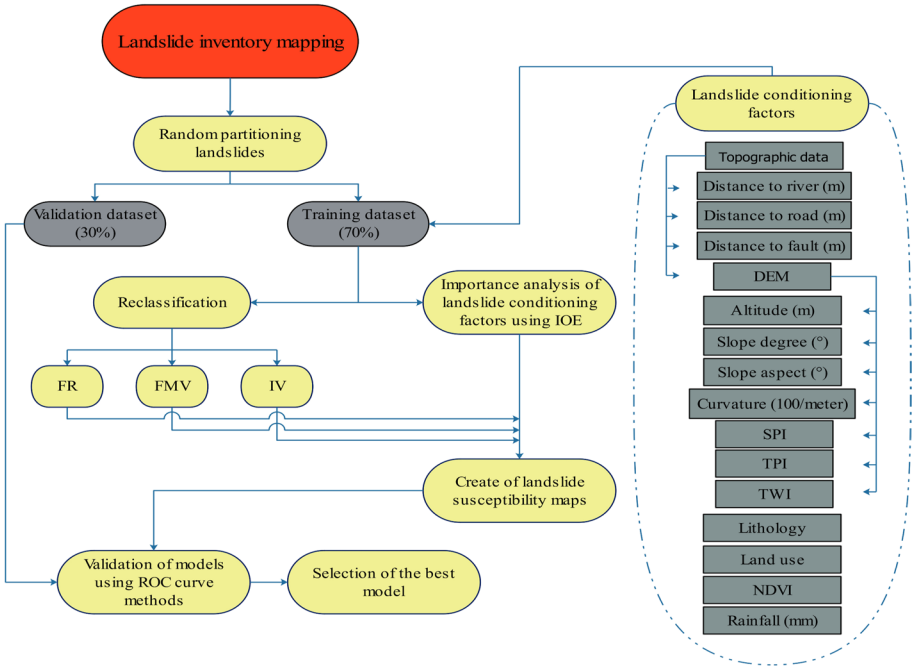

Fig. 4 Methodology flow chart for LSM

3.2 Fuzzy membership value (FMV)

Fuzzy logic shows a grey look into the actual world, finding a way to draw the external fact. For a sample, if white is represented by 1 and black by 0, then grey will be a number which will be between 1 and 0 (Abedi Gheshlaghi and Feizizadeh 2017). Various techniques have been suggested to implement fuzzy principles. One of the techniques of executing this is by utilizing the FR. After the calculation of the FR, the values acquired by making use of the equation given below were normalized, and fuzzy membership values (FMVs) were obtained.

$$\mu_{ij} = \mathrm{FR}_{ij}/max_i(\mathrm{FR}_{ij}) \tag{6}$$

where μ_{ij} is the FMV of class i of parameter j.

3.3 Information value (IV)

It is a bivariate statistical method for the spatial forecasting of an event based on the parameter and occurrence relationship. Until now IV has been the most useful model for the mapping of landslide susceptibility by determining the impact of factors governing landslide events happening in the region under study (Achour et al. 2017). A negative value of I_i shows that the probability of a landslide occurrence is less than average, whereas a positive value of I_i exhibits that the probability of a landslide occurrence is maximum than average. The IV I_i for a parameter i can be computed using the equation given below:

$$I_i = \log_2 \frac{A_i/B_i}{A/B} \tag{7}$$

where I_i is the information value, A_i represents the landslides number containing parameter class i, B_i shows the area of parameter class i, A exhibits the whole number of landslides, and B manifests the total of the study region.

3.4 Index of entropy (IOE)

Index of entropy is the evaluation of the uncertainty of a system (Al-Abadi et al. 2016). Researchers, i.e. Kornejady and Pourghasemi (Kornejady and Pourghasemi 2019) and Sharma et al. (Sharma et al. 2015), employed the IOE model for the susceptibility of landslides in various parts of the globe. IOE allows approximating the weight for every landslide conditioning factor (W_j) utilizing the equations given below (Bednarik et al. 2010):

$$P_{ij} = \frac{a}{b} \tag{8}$$

$$(P_{ij}) = \frac{P_{ij}}{\sum_{i=1}^{S_J} P_{ij}} \tag{9}$$

where b is the percentage of the pixels in a class to the whole pixels; a is the percentage of landslide happening pixels in a class to the total landslide happening pixels; (P_{ij}) is the probability density.

$$H_j = -\sum_{i=1}^{S_J} (P_{ij}) \log_2 (P_{ij}). j = 1.2. \ldots n \tag{10}$$

$$H_{jmax} = \log_2 S_j \tag{11}$$

where H_j *and* H_{jmax} are the entropy values; S_j is the number of classes.

$$I_j = \frac{H_{jmax} - H_j}{H_{jmax}}. I = (0.1). j = 1.2. \ldots .n \tag{12}$$

$$W_j = I_j P_{ij} \tag{13}$$

where W_j is the weight value of the factor as a whole; and I_j is the value of information coefficient.

3.5 Methods integration

To integrate the techniques, the landslide susceptibility index (LSI) is computed, on the basis of weights and rating values to all categories of the distinct conditioning factors which represent the association between classes in a parameter, and the weight values of every parameters (Table 4). Therefore, the final maps of LSI were created making use of the equations given as:

$$\mathrm{LSI}_{FMV-IOE} = \sum_{j=1}^{n} \mathrm{FMV}_{ij} W_j \tag{14}$$

$$\mathrm{LSI}_{FR-IOE} = \sum_{j=1}^{n} \mathrm{FR}_{ij} W_j \tag{15}$$

$$\mathrm{LSI}_{IV-IOE} = \sum_{j=1}^{n} \mathrm{IV}_{ij} W_j \tag{16}$$

where $\mathrm{LSI}_{FMV-IOE}$,LSI_{FR-IOE}, and LSI_{IV-IOE} are the susceptibility indexes of the landslide, FMV_{ij} is the weight of class i in factor j, FR_{ij} is the weight of class i in factor j, IV_{ij} is the weight of class i in factor j, W_j the weight of factor and n is the number of factors.

LSI shows the landslide susceptibility on the basis of the number of factors (parameters), weight of the classes of every factor, and weight of every factor in the final susceptibility analysis (Fig. 5).

3.6 Performance and validation of model

To understand the significance of the model outputs, validation of the techniques is an essential step in any modelling process (Balamurugan et al. 2016). In this research, the relative operating characteristics (ROC) curve was employed to analyse the models' performance. The ROC curve is designed in a two-dimensional space in which the Y-axis denotes specificity (the number of non-landslide pixels accurately classified as non-landslide), and the X-axis specifies sensitivity (the number of pixels of landslide accurately classified as a landslide). As an integral section of the ROC curve, the area under the receiver operating characteristic (AUROC) was employed to assess the landslide models' performance. In the AUROC, the graph depicts the rate of false-positive (1 − specificity) on the X-axis (Eq. 14) and the rate of true-positive (sensitivity) on the Y-axis (Eq. 15):

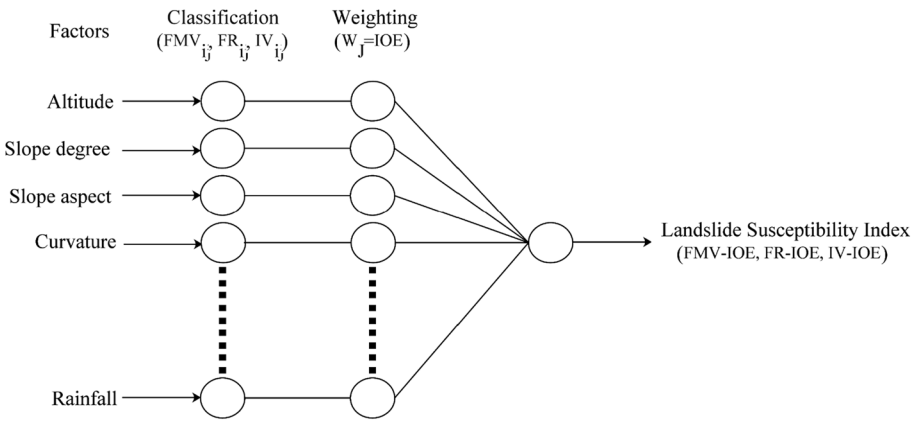

Fig. 5 Integration of methods for LSI

$$X = 1 - \text{specificity} = 1 - \left[\frac{\text{TN}}{\text{TN} + \text{FP}}\right] \tag{17}$$

$$Y = \text{sensitivity} = \left[\frac{\text{TP}}{\text{TP} + \text{FN}}\right] \tag{18}$$

where FP is false-positive, TN is true-negative,*FN* is false-negative, and TP is true-positive (Arabameri et al. 2019a). The AUROC and prediction accuracy quantitative–qualitative correlation, which ranges from 0 to 1, are described as follows: excellent (0.9–1), very good (0.8–0.9), good (0.7–0.8), moderate (0.6–0.7), and weak (0.5–0.6) (Arabameri et al. 2019b).

In addition to this, statistical indexes such as specificity, sensitivity, and accuracy were utilized to assess the ensemble techniques performance. The proportion of pixels accurately classified as occurrences of landslide is known as sensitivity. On the other hand, the proportion of non-landslides pixels accurately as non-landslides is known as specificity. The proportion of pixels of landslide and non-landslide which are accurately classified is known as accuracy (Chen et al. 2018). These terms can be computed utilizing the equations given below:

$$\text{Sensitivity} = \frac{TP}{TP + FN} \tag{19}$$

$$\text{Specificity} = \frac{TN}{TN + FP} \tag{20}$$

$$\text{Accuracy} = \frac{TP + TN}{TP + TN + FP + FN} \tag{21}$$

where TN (true-negative) and TP (true-positive) represent the number of pixels which are correctly classified and FN (false-negative) and FP (false-positive) represent the number of pixels which are incorrectly classified.

4 Results

The significant step in the prevention of landslides in the landslide-vulnerable areas is the LSM (Abedi Gheshlaghi and Feizizadeh 2017). The maps of landslide susceptibility were prepared after the completion of training process of landslide techniques in three major stages such as (i) preparation of factors (ii) generation of landslide susceptibility indexes (LSIs), and (iii) reclassification of LSIs. During the first step, the techniques, that is, FMV, IV, and FR, were employed for the derivation of the sub-criteria weights, and IOE technique was computed for the derivation of criteria weights (Table 4). During the second step, a set of whole sampling pixels were used for the generation of LSIs of all pixels in the whole study region. During the third stage, making use of the natural break technique the LSIs has been reclassified. On the basis of this approach, the reclassification of LSIs has been done into five susceptible levels such as very high, high, moderate, low, and very low (Fig. 7).

4.1 Importance analysis of landslide parameters

Fourteen landslide parameters predictive capability is presented in Fig. 6 while utilizing the IOE method. Of these, altitude has the maximum value of all (W_j= 1.343), followed by lithology (W_j=0.641), slope degree (W_j=0.321), NDVI W_j (=0.315), rainfall (W_j=0.295), TWI (W_j=0.274), SPI (W_j=0.259), distance to road (W_j=0.210), distance to fault (W_j =0.160), slope aspect (W_j=0.159), land use (W_j=0.143), distance to river (W_j=0.081), TPI (W_j=0.061), and curvature(W_j=0.037) (Table 4).

The results of multicollinearity test (Table 3) show that no significant multicollinearity was noted between the landslide conditioning factors. The minimum TOL was computed for lithology (0.242) as well as for the runoff height (0.397) which are, however, maximum than the theoretical critical value (0.10) for the confirmation of collinearity. Also, for all parameters the values of VIF are below the threshold of theoretical multicollinearity (b5.00). Therefore, these conditioning factors were all selected as input layers to create the maps of landslide susceptibility, because they make significant contribution to the occurrences of landslides on the basis of IOE and the assessment of multicollinearity in the study region.

4.2 Integration of the FMV and IOE methods

The relationship between landslides and every landslide associated parameter are summarized in Table 4. Higher FMV values show the maximum chances of landslide occurrence.

The obtained FMV values were employed as inputs to run the method of IOE. The LSI values were from 0.217 to 3.961. Finally, the LSM was obtained from the FMV_IOE method, which was categorized into five levels of landslide susceptibility: very high (2.597–3.961), high (1.648–2.597), moderate (1.272–1.648), low (0.918–1.272), and very low (0.217–0.918) (Fig. 7a).

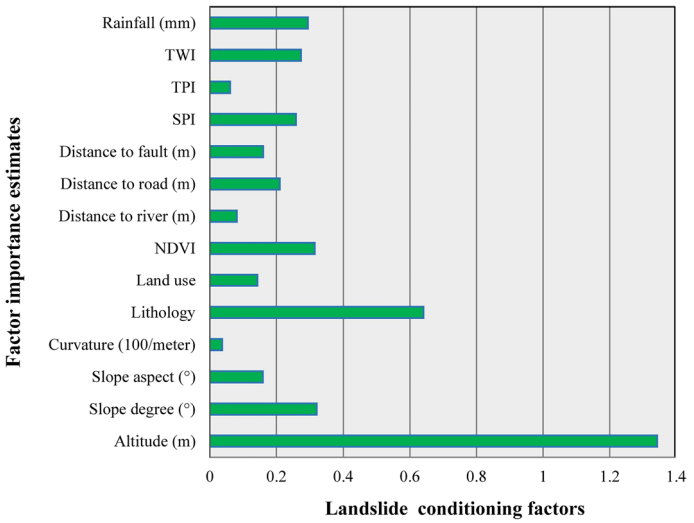

Fig. 6 Analysis of factor importance using IOE method

Table 3 Multicollinearity assessment for conditioning factors

Conditioning Factors	TOL	VIF
Altitude (m)	0.832	1.202
Slope degree (°)	0.564	1.773
Slope aspect (°)	0.694	1.441
Curvature (100/meter)	0.751	1.332
Lithology	0.611	1.637
Land use	0.397	2.519
NDVI	0.788	1.269
Distance to river (m)	0.282	3.546
Distance to road (m)	0.797	1.255
Distance to fault (m)	0.488	2.049
SPI	0.712	1.404
TPI	0.575	1.739
TWI	0.722	1.385
Rainfall (mm)	0.521	1.919

4.3 Integration of the FR and IOE methods

The correlations between landslides and every parameter making use of the FR method are summarized in Table 4. Overall, greater chances of landslide occurrence are manifested by the FR larger values.

To run the IOE method, the acquired values of FR were also employed as inputs. The range of measured LSI values was from 0.472 to 33.314. Finally, the LSM for the case of FR_IOE method was obtained, and was separated into five levels of landslide susceptibility: very high (12.565–33.314), high (7.791–12.565), moderate (4.413–7.791), low (2.399–4.413), and very low (0.472–2.399) (Fig. 7b).

4.4 Integration of the IV and IOE methods

The relationship between every landslide associated factor and landslides is summarized in Table 4. The IV larger values of exhibit maximum likelihood of landslide occurrence.

The acquired values of IV were also taken into account as inputs for running the IOE method. The range of computed LSI values was from −1.674 to 2.847. Finally, the LSM for the case of IV_IOE method was obtained, and the study region was dissected into five levels of landslide susceptibility: very high (1.543–2.847), high (0.441–1.543), moderate ((−0.132)–0.441), low ((−0.617)–(−0.132)), and very low ((−1.674)–(−0.617)) (Fig. 7c).

4.5 Percentage and density of susceptibility levels

Figure 8 presents the percentages of landslide susceptibility groups for every model. According to the FMV_IOE results, 1.86% of the entire region was observed in the very high susceptibility level, 13.98% in the high level, 28.22% in the moderate level, 29.13% in the low level, and 26.81% in the level of very low susceptibility. As for the FR_IOE ensemble, the low, very low, moderate, high, and very high levels were considered for the

Table 4 Spatial correlations between each landslide related parameter and landslides by the FR, the FMV, and the IOE methods

Parameter	Class	No. of pixels in domain	No. of landslide pixels	FMV	IV	$FR = P_{ij}$	(P_j)	H_j	H_j max	I_j	P_j	W_j
	1239–1500	17,682	0	0.000	0.000	0.000	0.000					
	1500–2000	17,391	7	0.043	−0.363	0.434	0.116					
Altitude (m)	2000–2500	15,089	20	0.140	0.155	1.428	0.264	1.309	2.322	0.436	3.078	1.343
	2500–3000	4819	8	0.330	0.253	1.789	0.423					
	> 3000	1059	17	1.000	1.238	17.298	0.506					
	0–5	17,079	2	0.054	−0.899	0.126	0.024					
	5–15	22,376	20	0.410	−0.016	0.963	0.180					
Slope degree (°)	15–25	12,427	22	0.811	0.280	1.907	0.357	1.625	2.322	0.300	1.070	0.321
	25–35	3665	8	1.000	0.372	2.352	0.440					
	> 35	493	0	0.000	0.000	0.000	0.000					
	Flat	1604	0	0.000	0.000	0.000	0.000					
	North	8893	18	1.000	0.339	2.181	0.325					
	Northeast	6231	5	0.396	−0.063	0.865	0.129					
	East	3142	1	0.157	−0.465	0.343	0.051					
Slope aspect (°)	Southeast	2686	0	0.000	0.000	0.000	0.000	2.493	3.170	0.214	0.745	0.159
	South	4995	1	0.099	−0.666	0.216	0.032					
	Southwest	8215	10	0.601	0.118	1.312	0.196					
	West	10,384	12	0.571	0.095	1.245	0.186					
	Northwest	9890	5	0.250	−0.264	0.545	0.081					
	Concave	27,901	30	1.000	0.064	1.159	0.454					
Curvature (100/meter)	Flat	2044	1	0.455	−0.278	0.527	0.206	1.516	1.585	0.043	0.851	0.037
	Convex	26,095	21	0.749	−0.062	0.867	0.340					
	Q^{sd}	7639	0	0.000	0.000	0.000	0.000					
	Ng^{ct}	234	0	0.000	0.000	0.000	0.000					
	PLQ^{ash}	7810	11	0.167	0.181	1.517	0.124					
	PLQ^{d}	19,691	22	0.132	0.081	1.204	0.099					

Table 4 (continued)

Parameter	Class	No. of pixels in domain	No. of landslide pixels	FMV	IV	FR = P_{ij}	(P_j)	H_j	H_j max	I_j	P_j	W_j
	Q^{tr}	84	0	0.000	0.000	0.000	0.000					
	Q^2	1352	0	0.000	0.000	0.000	0.000					
Lithology	Ng^b	446	0	0.000	0.000	0.000	0.000	1.171	3.700	0.684	0.938	0.641
	Q^3	309	0	0.000	0.000	0.000	0.000					
	J^l	215	0	0.000	0.000	0.000	0.000					
	J^d	125	0	0.000	0.000	0.000	0.000					
	K^l_l	7420	0	0.000	0.000	0.000	0.000					
	JK_l	8822	3	0.040	−0.436	0.367	0.030					
	K^c_l	1893	16	1.000	0.959	9.103	0.747					
	Agricultural land	13,189	15	1.000	0.088	1.226	0.403					
	Orchard land	2967	1	0.297	−0.439	0.364	0.120					
Land use	Grass land	32,805	34	0.911	0.048	1.117	0.367	1.775	2.322	0.235	0.608	0.143
	Barren land	6463	2	0.272	−0.477	0.334	0.110					
	Cultivation and built−up area	616	0	0.000	0.000	0.000	0.000					
	(−0.09)–0.2	46,871	42	0.659	−0.015	0.966	0.397					
NDVI	0.2–0.4	7357	10	1.000	0.166	1.465	0.603	0.969	1.585	0.388	0.810	0.315
	> 0.4	1812	0	0.000	0.000	0.000	0.000					
	0–200	12,527	9	0.340	−0.111	0.774	0.140					
	200–400	8788	7	0.377	−0.066	0.859	0.156					
Distance to river (m)	400–600	7815	6	0.363	−0.082	0.827	0.150	2.152	2.322	0.073	1.104	0.081
	600–800	7572	16	1.000	0.357	2.278	0.413					
	> 800	19,338	14	0.343	−0.108	0.780	0.141					
	0–200	10,498	1	0.058	−0.989	0.103	0.038					
	200–400	6546	0	0.000	0.000	0.000	0.000					
Distance to road (m)	400–600	5399	2	0.227	−0.399	0.399	0.147	1.420	2.322	0.388	0.542	0.210

Table 4 (continued)

Parameter	Class	No. of pixels in domain	No. of landslide pixels	FMV	IV	FR = P_{ij}	(P_j)	H_j	H_j max	I_j	P_j	W_j
	600–800	4805	2	0.255	−0.348	0.449	0.166					
	> 800	28,792	47	1.000	0.245	1.759	0.649					
	0–1000	2501	6	0.929	0.413	2.587	0.287					
	1000–2000	4623	6	0.502	0.146	1.399	0.155					
Distance to fault (m)	2000–3000	6190	16	1.000	0.445	2.785	0.309	2.115	2.322	0.089	1.800	0.160
	3000–4000	6926	12	0.671	0.271	1.867	0.207					
	> 4000	35,800	12	0.130	−0.442	0.361	0.040					
	(−4.6)–(−1.5)	3623	1	0.126	−0.527	0.067	0.262					
	(−1.5)–0	7740	17	1.000	0.374	0.537	0.482					
SPI	0–2	23,445	25	0.485	0.060	0.261	0.506	1.640	2.322	0.294	0.882	0.259
	2–4.5	16,266	9	0.252	−0.224	0.135	0.390					
	> 4.5	4966	0	0.000	0.000	0.000	0.000					
	(−106.7)–(−34.5)	4855	7	0.849	0.192	1.554	0.238					
	(−34.5)–(−9.28)	12,053	11	0.537	−0.007	0.983	0.151					
TPI	(−9.28)–14	26,401	13	0.290	−0.275	0.531	0.081	2.213	2.322	0.047	1.305	0.061
	14–47.48	9413	16	1.000	0.263	1.832	0.281					
	> 47.48	3318	5	0.887	0.211	1.624	0.249					
	(−0.5)–2	19,819	22	0.898	0.078	0.355	0.530					
	2–4	20,236	25	1.000	0.124	0.396	0.529					
TWI	4–6	10,522	3	0.231	−0.513	0.091	0.315	1.375	2.322	0.408	0.673	0.274
	6–9	4065	2	0.398	−0.275	0.158	0.000					
	> 9	1398	0	0.000	0.000	0.000	0.000					
	221–227	9919	4	0.121	−0.362	0.435	0.070					
	227–230	13,308	6	0.135	−0.314	0.486	0.078					
Rainfall (mm)	230–234	16,431	8	0.146	−0.280	0.525	0.085	1.769	2.322	0.238	1.241	0.295

Table 4 (continued)

Parameter	Class	No. of pixels in domain	No. of landslide pixels	FMV	IV	$FR = P_{ij}$	(P_j)	H_j	H_j max	I_j	P_j	W_j
	234–239	9170	10	0.328	0.070	1.175	0.189					
	> 239	7212	24	1.000	0.555	3.586	0.578					

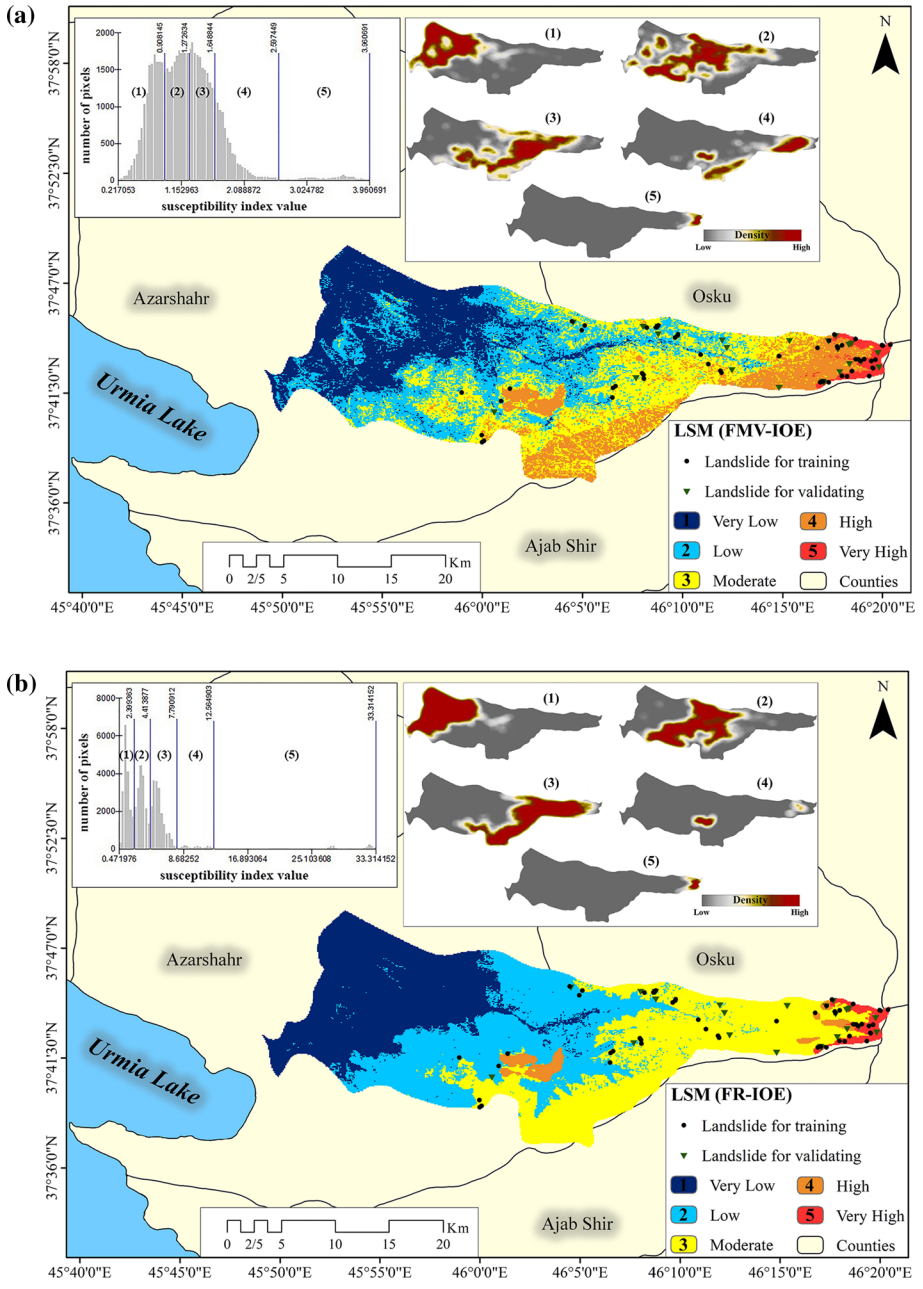

Fig. 7 LSMs using: **a** FMV_IOE; **b** FR_IOE; **c** IV_IOE

percentage values of 31.6, 31.42, 32.86, 2.32, and 1.8%, respectively. Correspondingly in the IV_IOE ensemble, 41.1, 20.24, 25.98, 10.89, and 1.79% of the region under study were assigned to low, very low, moderate, high, and very high susceptible to landslide respectively.

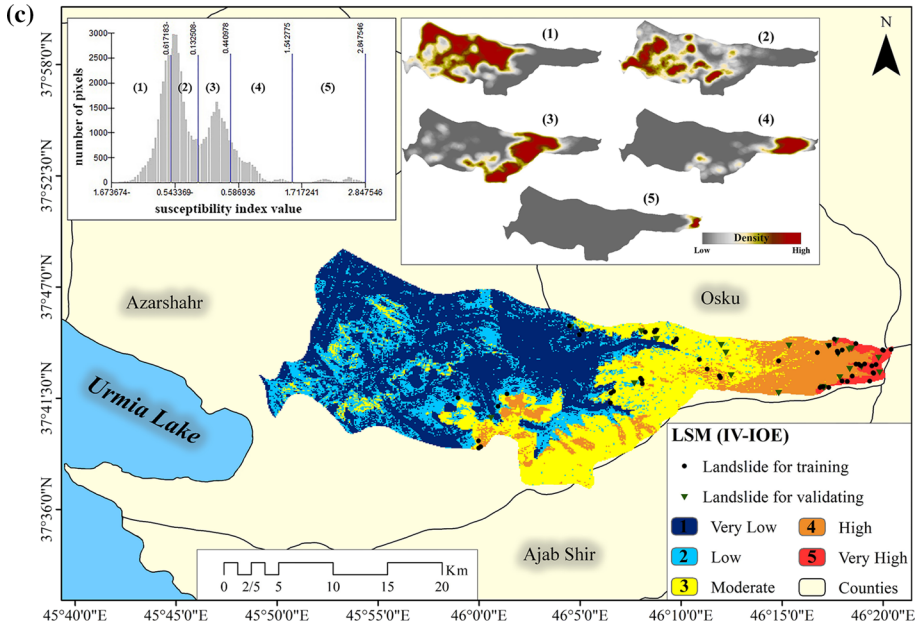

Fig. 7 (continued)

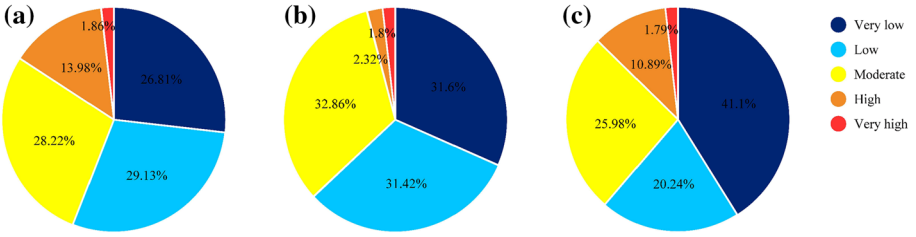

Fig. 8 Distribution of the different susceptibility levels for **a** FMV_IOE, **b** FR_IOE, and **c** IV_IOE methods

To assess the performance of the three LSMs, the landslide density (LD) was also computed (Table 5) which is a ratio of the percentage of landslide pixels and the percentage of the level pixels on every susceptible level (Pham et al. 2016). In the reliable LSMs, the levels of maximum susceptibility should indicate maximum LD.

The findings indicated that the LD value changed among the levels the ranging from 0 to 17.88 (Table 5). In each map, the level of very low susceptibility had the minimum LD values, followed by the level of low susceptibility, level of moderate susceptibility, level of high susceptibility, and level of very high susceptibility. The findings also manifested that the FMV_IOE technique had the maximum LD for the very high susceptibility level and showed good performance than the other two techniques.

Figure 8 manifests the density of LSI maps in every individual level of landslide susceptibility. In the context of the FMV_IOE model, the density was highest to low, very low, moderate, high, and very high susceptibility levels in northwest, central, southeast, eastern, and eastern regions, respectively. In this context, in the FR_IOE model, the density

Table 5 Landslide density within the LSMs

Methods	Susceptibility levels	% of pixels in levels	% of landslides in levels	LD
	Very high	1.86	33.33	17.88
	High	13.98	26.67	1.91
FMV-IOE	Moderate	28.22	30.67	1.09
	Low	29.13	9.33	0.32
	Very low	26.81	0	0
	Very high	1.8	30.67	17.06
	High	2.32	5.33	2.3
FR-IOE	Moderate	32.86	48	1.46
	Low	31.42	16	0.51
	Very low	31.6	0	0
	Very high	1.79	28	15.65
	High	10.89	25.33	2.33
IV-IOE	Moderate	25.99	33.33	1.28
	Low	20.24	13.33	0.66
	Very low	41.1	0	0

was higher to low, very low, moderate, high, and very high susceptibility levels in western, central, northeast, southern, and eastern regions, respectively. For the IV_IOE model, the density was maximum to low, very low, moderate, high, and very high susceptibility levels in northwest, southwest, southeast, eastern, and eastern regions, respectively (Abedi Gheshlaghi et al. 2020a, b).

4.6 Integrated techniques assessment

Tables 6 and 7 show the general assessment of the landslide susceptibility methods while making use of ROC curves with training and validation datasets.

The AUROC values in integrated methods were significant statistically due to having Std. error to 0.018 (less than 0.05). For the ease of interpretation, the performance of methods was overlaid on a single graphic ROC (Fig. 9a and b). The acquired output for the training phase manifests that the values of AUROC for FMV_IOE, FR_IOE were rather similar to value 0.930 and 0.929, respectively, whereas the AUROC value of IV_IOE (0.926) was lower than it models. Also, the validation of the three achieved maps revealed that values of AUROC for FMV_IOE, FR_IOE with values close to one other (0.927 and

Table 6 AUROC analysis for the ensemble methods with the training dataset

Methods	AUROC	SE	Asymptotic 95% confidence interval	
			Lower-bound	Upper-bound
FR-IOE	0.929	0.018	0.894	0.964
FMV-IOE	0.930	0.018	0.895	0.965
IV-IOE	0.926	0.018	0.891	0.961

Table 7 AUROC analysis for the ensemble methods with the validation dataset

Methods	AUROC	SE	Asymptotic 95% confidence interval	
			Lower-bound	Upper-bound
FR-IOE	0.925	0.018	0.890	0.960
FMV-IOE	0.927	0.018	0.892	0.962
IV-IOE	0.918	0.019	0.882	0.955

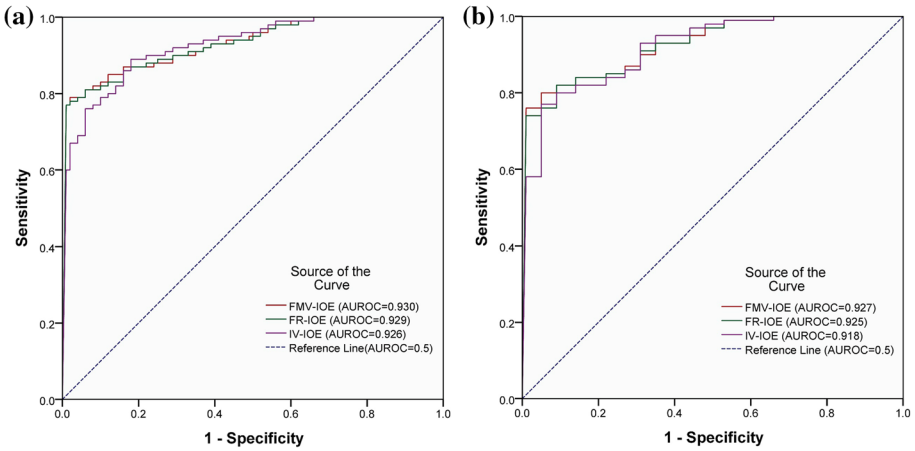

Fig. 9 **a** ROC curve and AUROCs of the training dataset and **b** ROC curve and AUROCs of the validation dataset

0.925, respectively) had a better degree of fit with the training database, while IV_IOE with AUROC value (0.918) was lower than it models. Therefore, based on the acquired results, IV_IOE model in both training and validation phases has the lower that it models. On the other hand, FMV_IOE, FR_IOE were rather similar, but the FMV_IOE was more efficient in the process of modelling using the dataset for training. Therefore, the FMV_IOE can be utilized as a propitious technique to develop the study region's landslide susceptibility map.

Statistical indexes were used to perform the additional training and validation of the datasets for the three models (Tables 8 and 9).

The landslides techniques performance employing statistical index-based training dataset is exhibited in Table 8. Here, the FMV_IOE method manifests the highest performance for the landslides pixels' classification (sensitivity = 96.2%), followed by the FR_IOE method (sensitivity = 94.2%), and the IV_IOE method (sensitivity = 90.4%). The classification of non-landslide pixels was shown by the highest performance of the FMV_IOE method (specificity = 90.4%), followed by the FR_IOE method (specificity = 88.5%), and the IV_IOE method (specificity = 86.5%). The highest accuracy is of FMV_IOE method with 93.3% value, followed by the FR_IOE method (91.3%), and the IV_IOE method (88.5%). The landslides techniques validation making use of statistical indexes based dataset for validation is represented in Table 9. The highest performance is of FMV_IOE method for the landslide pixels' classification (sensitivity = 95.7%), followed

Table 8 The performance of techniques using the training dataset

Evaluation parameters	Methods		
	FMV-IOE	FR-IOE	IV-IOE
True-positive	50	49	47
True-negative	47	46	45
False-positive	5	6	7
False-negative	2	3	5
Sensitivity (%)	96.2	94.2	90.4
Specificity (%)	90.4	88.5	86.5
Accuracy (%)	93.3	91.3	88.5

Table 9 Methods performance using the validation dataset

Evaluation parameters	Methods		
	FMV-IOE	FR-IOE	IV-IOE
True-positive	22	21	20
True-negative	20	20	19
False-positive	3	3	4
False-negative	1	2	3
Sensitivity (%)	95.7	91.3	87.0
Specificity (%)	87.0	87.0	82.6
Accuracy (%)	91.3	89.1	84.8

by the methods such as FR_IOE method (sensitivity = 91.3%), and IV_IOE method (sensitivity = 87%). For the non-landslides pixels' classification, the better performance is of the FMV_IOE method (specificity = 87%), followed by the other two methods such as FR_IOE method (specificity = 87%), and the IV_IOE method (specificity = 82.6%). The FMV_IOE method showed better performance with the maximum value of 91.3%, followed by the methods that are FR_IOE method (89.1%), and the IV_IOE method (84.8%). As a whole, all the three landslide ensemble techniques are appropriate for LSM in the ACB, and out of all the FMV_IOE technique shows the most stable and best performance in the ACB.

5 Discussion

The LSMs is generally considered the first stage in dealing with landslide hazard mitigation. Hence, the preparation of a high-precision LSM can be useful in the field of hazard management. Hitherto, several approaches have been developed for LSMs to obtain the best method for a given area. Therefore, it is necessary to investigate novel techniques for LSA (Abedi Gheshlaghi and Feizizadeh 2017). In comparison with conventional approaches, i.e. FMV, FR, IV, and IOE methods which are familiar in solving many real-world problems, recently, researchers around the world have designed various models utilizing integrated techniques to various scientific topics (Abedi Gheshlaghi and Valizadeh Kamran 2018; Ferrari et al. 2018; Hong and Lee 2019; Wagner and Fohrer 2019; Abedi Gheshlaghi et al. 2020a,

b; Feizizadeh et al. 2020). Ensemble models are showing promising and premier techniques to solve complex problems. Our study performs a comparison to evaluate the performances of some ensemble models (FMV_IOE, FR_IOE, and IV_IOE) in identifying landslide-prone areas. The most important contribution of the present study is the simultaneous use of fuzzy system and bivariate statistics, and the integration of their results along for LSA.

Because of the limitations of each zoning approach, the models were combined and integrated to improve their performance. Among the individual techniques, the FMV method had a higher predictive accuracy than the rest of the individual techniques, as already pointed out by previous studies (Sahana and Sajjad 2017; Ozdemir 2020). The combination of the individual techniques increased their accuracy, which was also associated with previous research (Nguyen et al. 2019; Chen and Li 2020; Pham et al. 2020). Among the ensemble models, the combination of fuzzy system and bivariate statistics approaches was more efficient than the rest of the technique combinations, which was in associated with previous studies (Hong et al. 2017).

An important and fundamental step in any LSM process is identifying the most significant factors in landslide assessment (Abedi Gheshlaghi and Feizizadeh 2017). To achieve this aim, we selected 14 conditioning factors (altitude, slope aspect, slope degree, lithology, distance to fault, curvature, land use, distance to river, TPI, TWI, SPI, NDVI, distance to road, and rainfall) for modelling. To test the contribution of these influencing parameters to the landslide methods, the IOE technique has been employed. The IOE technique is efficient to show high predictive proficiency parameters. Of these 14 factors, altitude and lithology contributed most to the models, whereas curvature and TPI contributed least. These results are in line with other previous works and studies (Ercanoglu and Temiz 2011; Du et al. 2017), especially things that are done in Iranian environments (Devkota et al. 2013; Jaafari et al. 2014).

The prediction power of the best-integrated methods was graphically determined to make use of the ROC curve (Fig. 9) and statistical measures (Tables 8 and 9). The maximum AUROC and statistical measures values among the integrated methods were acquired by the FMV-IOE (AUROC = 0.927, sensitivity = 95.7%, specificity = 87%, accuracy = 91.3%). Although in all three maps, the landslides are not present in the level of very low susceptibility, the findings exhibited more values (19.78) of LD in the very high and high levels of the FMV_IOE map, while they are less in the FR_IOE (19.35) and IV_IOE (17.98) maps (Table 5). This indicates that the FMV_IOE ensemble model showed best performance than the mentioned two models.

In general, all three landslide ensemble methods have given best performance for LSM, but the FMV_IOE model has given the comparatively excellent performance. To emphasize the relevance of the results obtained in the present study, it is important to note that in the literature dealing with LSA, a small number of analyses report AUROC values higher than 0.9 (e.g. Abedini et al. 2018; Pham et al. 2019).

The ensemble models proposed here successfully improved the accuracy of LSM by 20% compared to previous studies that used individual techniques for the study area (Rajabi et al. 2016). Therefore, this study constitutes a step forward in the field of accurate prediction of natural hazards by suggesting that ensemble models.

6 Conclusions

To alleviate the devastating impacts of landslides, modelling, and creating precise LSMs is essential. The techniques suggested in this research are three hybrid intelligent approaches (FMV_IOE, FR_IOE, and IV_IOE) for the mapping of landslide susceptibility. The ACB, East Azerbaijan province of Iran, was the case study for which the techniques were utilized. It was developed employing 52 (training data) and validated with 23 (validation data) locations of landslide and fourteen parameters, which includes altitude, curvature, slope aspect, slope degree, lithology, NDVI, land use, distance to faults, distance to rivers, distance to roads, SPI, TWI, TPI, and rainfall. Investigation of the spatial impact of every parameter on the occurrence of landslide showed the altitude, lithology, slope degree, and NDVI as the most effective factors.

The comparison indicated that though all three methods were applicable for landslide modelling, the FMV_IOE method generated higher accuracy of prediction. Therefore, the FMV_IOE can be used as a propitious method to create the landslide susceptibility map in the ACB. We propose that this evolutionary approach (FMV_IOE) can be employed for other areas with homogeneous (similar) conditioning factors. The generated susceptibility maps can assist the governments, planners, and managers to offer a better way for the management of slope and planning of land use in order to manage the hazard associated risks and mitigate further damage.

As the final conclusion, integrated models are suggested for landslide mapping because of their more stable results, higher prediction accuracy, and more generalization ability. Nevertheless, there is limited literature on the utilization of integrated approaches in landslide mapping, and thus, the development of other integrated frameworks is strongly recommended. The proposed approach is a promising tool that can be applied in other types of natural hazard modelling such as wildfire, gully erosion, land subsidence, and flood. From this, it is apparent that a more accurate susceptibility map can decrease the damage and cost from natural hazards.

Data availability This work does not have any data.

Declarations

Conflict of interest The authors declare that they have no conflict of interest.

References

Abedi Gheshlaghi H (2019) Using GIS to develop a model for forest fire risk mapping. J Indian Soc Remote Sens 47:1173–1185. https://doi.org/10.1007/s12524-019-00981-z

Abedi Gheshlaghi H, Feizizadeh B (2017) An integrated approach of analytical network process and fuzzy based spatial decision making systems applied to landslide risk mapping. J African Earth Sci 133:15–24. https://doi.org/10.1016/j.jafrearsci.2017.05.007

Abedi Gheshlaghi H, Valizadeh Kamran K (2018) Evaluation and zoning of forest fire risk using multi-criteria decision-making techniques and GIS. J Nat Environ Hazards 15:49–66. https://doi.org/10.22111/JNEH.2017.3204

Abedi Gheshlaghi H, Feizizadeh B, Blaschke T (2020a) GIS-based forest fire risk mapping using the analytical network process and fuzzy logic. J Environ Plan Manag 63:481–499. https://doi.org/10.1080/09640568.2019.1594726

Abedi Gheshlaghi H, Feizizadeh B, Blaschke T et al (2020b) Forest fire susceptibility modeling using hybrid approaches. Trans GIS. https://doi.org/10.1111/tgis.12688
Abedini M, Ghasemian B, Shirzadi A et al (2018) A novel hybrid approach of bayesian logistic regression and its ensembles for landslide susceptibility assessment. Geocarto Int. https://doi.org/10.1080/10106049.2018.1499820
Achour Y, Boumezbeur A, Hadji R et al (2017) Landslide susceptibility mapping using analytic hierarchy process and information value methods along a highway road section in Constantine. Algeria Arab J Geosci 10:194. https://doi.org/10.1007/s12517-017-2980-6
Aditian A, Kubota T, Shinohara Y (2018) Comparison of GIS-based landslide susceptibility models using frequency ratio, logistic regression, and artificial neural network in a tertiary region of Ambon, Indonesia. Geomorphology 318:101–111. https://doi.org/10.1016/j.geomorph.2018.06.006
Al-Abadi AM, Al-Temmeme AA, Al-Ghanimy MA (2016) A GIS-based combining of frequency ratio and index of entropy approaches for mapping groundwater availability zones at Badra–Al Al-Gharbi–Teeb areas, Iraq. Sustain Water Resour Manag 2:265–283. https://doi.org/10.1007/s40899-016-0056-5
Alimohammadlou Y, Najafi A, Yalcin A (2013) Landslide process and impacts: A proposed classification method. CATENA 104:219–232. https://doi.org/10.1016/j.catena.2012.11.013
Alvioli M, Melillo M, Guzzetti F et al (2018) Implications of climate change on landslide hazard in Central Italy. Sci Total Environ 630:1528–1543. https://doi.org/10.1016/j.scitotenv.2018.02.315
Arabameri A, Rezaei K, Cerdà A et al (2019a) A comparison of statistical methods and multi-criteria decision making to map flood hazard susceptibility in Northern Iran. Sci Total Environ 660:443–458. https://doi.org/10.1016/j.scitotenv.2019.01.021
Arabameri A, Yamani M, Pradhan B et al (2019b) Novel ensembles of COPRAS multi-criteria decision-making with logistic regression, boosted regression tree, and random forest for spatial prediction of gully erosion susceptibility. Sci Total Environ 688:903–916. https://doi.org/10.1016/j.scitotenv.2019.06.205
Arabameri A, Pradhan B, Rezaei K et al (2020) An ensemble model for landslide susceptibility mapping in a forested area. Geocarto Int 35:1680–1705. https://doi.org/10.1080/10106049.2019.1585484
Ayalew L, Yamagishi H (2005) The application of GIS-based logistic regression for landslide susceptibility mapping in the Kakuda-Yahiko Mountains, Central Japan. Geomorphology 65:15–31. https://doi.org/10.1016/j.geomorph.2004.06.010
Bahrami Y, Hassani H, Maghsoudi A (2020) Landslide susceptibility mapping using AHP and fuzzy methods in the Gilan province Iran. GeoJournal. https://doi.org/10.1007/s10708-020-10162-y
Balamurugan G, Ramesh V, Touthang M (2016) Landslide susceptibility zonation mapping using frequency ratio and fuzzy gamma operator models in part of NH-39, Manipur, India. Nat Hazards 84:465–488. https://doi.org/10.1007/s11069-016-2434-6
Bednarik M, Magulová B, Matys M, Marschalko M (2010) Landslide susceptibility assessment of the Kraľovany-Liptovský Mikuláš railway case study. Phys Chem Earth Parts A/B/C 35:162–171. https://doi.org/10.1016/j.pce.2009.12.002
Bourenane H, Guettouche MS, Bouhadad Y, Braham M (2016) Landslide hazard mapping in the Constantine city, Northeast Algeria using frequency ratio, weighting factor, logistic regression, weights of evidence, and analytical hierarchy process methods. Arab J Geosci 9:154. https://doi.org/10.1007/s12517-015-2222-8
Bui DT, Pradhan B, Lofman O et al (2012) Spatial prediction of landslide hazards in Hoa Binh province (Vietnam): a comparative assessment of the efficacy of evidential belief functions and fuzzy logic models. CATENA 96:28–40. https://doi.org/10.1016/j.catena.2012.04.001
Bui DT, Ho TC, Revhaug I, et al (2014) Landslide susceptibility mapping along the national road 32 of Vietnam using GIS-based J48 decision tree classifier and its ensembles. In: Cartography from pole to pole. Springer, pp 303–317
Bui D, Tuan TA, Klempe H et al (2016) Spatial prediction models for shallow landslide hazards: a comparative assessment of the efficacy of support vector machines, artificial neural networks, kernel logistic regression, and logistic model tree. Landslides 13:361–378. https://doi.org/10.1007/s10346-015-0557-6
Bui DT, Hoang N-D, Nguyen H, Tran X-L (2019) Spatial prediction of shallow landslide using Bat algorithm optimized machine learning approach: a case study in Lang Son Province. Vietnam Adv Eng Informatics 42:100978. https://doi.org/10.1016/j.aei.2019.100978
Chen W, Li Y (2020) GIS-based evaluation of landslide susceptibility using hybrid computational intelligence models. CATENA 195:104777. https://doi.org/10.1016/j.catena.2020.104777
Chen W, Wang J, Xie X et al (2016) Spatial prediction of landslide susceptibility using integrated frequency ratio with entropy and support vector machines by different kernel functions. Environ Earth Sci 75:1344. https://doi.org/10.1007/s12665-016-6162-8

Chen W, Xie X, Peng J et al (2018) GIS-based landslide susceptibility evaluation using a novel hybrid integration approach of bivariate statistical based random forest method. CATENA 164:135–149. https://doi.org/10.1016/j.catena.2018.01.012

Chen W, Panahi M, Tsangaratos P et al (2019a) Applying population-based evolutionary algorithms and a neuro-fuzzy system for modelling landslide susceptibility. CATENA 172:212–231. https://doi.org/10.1016/j.catena.2018.08.025

Chen W, Sun Z, Han J (2019b) Landslide susceptibility modelling using integrated ensemble weights of evidence with logistic regression and random forest models. Appl Sci 9:171. https://doi.org/10.3390/app9010171

Choi KY, Cheung RWM (2013) Landslide disaster prevention and mitigation through works in Hong Kong. J Rock Mech Geotech Eng 5:354–365. https://doi.org/10.1016/j.jrmge.2013.07.007

Constantin M, Bednarik M, Jurchescu MC, Vlaicu M (2011) Landslide susceptibility assessment using the bivariate statistical analysis and the index of entropy in the Sibiciu Basin (Romania). Environ earth Sci 63:397–406. https://doi.org/10.1007/s12665-010-0724-y

Corominas J, van Westen C, Frattini P et al (2014) Recommendations for the quantitative analysis of landslide risk. Bull Eng Geol Environ 73:209–263. https://doi.org/10.1007/s10064-013-0538-8

Costache R, Bui DT (2019) Spatial prediction of flood potential using new ensembles of bivariate statistics and artificial intelligence: A case study at the Putna river catchment of Romania. Sci Total Environ 691:1098–1118. https://doi.org/10.1016/j.scitotenv.2019.07.197

CRED (2018) The human cost of natural disasters. a global perspective

Cruden DM (1991) A simple definition of a landslide. Bull Eng Geol Environ 43:27–29. https://doi.org/10.1007/BF02590167

Dang V-H, Dieu TB, Tran X-L, Hoang N-D (2019) Enhancing the accuracy of rainfall-induced landslide prediction along mountain roads with a GIS-based random forest classifier. Bull Eng Geol Environ 78:2835–2849. https://doi.org/10.1007/s10064-018-1273-y

Dehnavi A, Aghdam IN, Pradhan B, Varzandeh MHM (2015) A new hybrid model using step-wise weight assessment ratio analysis (SWARA) technique and adaptive neuro-fuzzy inference system (ANFIS) for regional landslide hazard assessment in Iran. CATENA 135:122–148. https://doi.org/10.1016/j.catena.2015.07.020

Devkota KC, Regmi AD, Pourghasemi HR et al (2013) Landslide susceptibility mapping using certainty factor, index of entropy and logistic regression models in GIS and their comparison at Mugling-Narayanghat road section in Nepal Himalaya. Nat Hazards 65:135–165. https://doi.org/10.1007/s11069-012-0347-6

Dou J, Yunus AP, Bui DT et al (2019) Assessment of advanced random forest and decision tree algorithms for modelling rainfall-induced landslide susceptibility in the Izu-Oshima Volcanic Island Japan. Sci Total Environ. https://doi.org/10.1016/j.scitotenv.2019.01.221

Du G, Zhang Y, Iqbal J et al (2017) Landslide susceptibility mapping using an integrated model of information value method and logistic regression in the Bailongjiang watershed, Gansu Province, China. J Mt Sci 14:249–268. https://doi.org/10.1007/s11629-016-4126-9

Ebrahimy H, Feizizadeh B, Salmani S, Azadi H (2020) A comparative study of land subsidence susceptibility mapping of Tasuj plane, Iran, using boosted regression tree, random forest and classification and regression tree methods. Environ Earth Sci 79:223. https://doi.org/10.1007/s12665-020-08953-0

Ercanoglu M, Temiz FA (2011) Application of logistic regression and fuzzy operators to landslide susceptibility assessment in Azdavay (Kastamonu, Turkey). Environ Earth Sci 64:949–964. https://doi.org/10.1007/s12665-011-0912-4

Farrokhnia A, Pirasteh S, Pradhan B et al (2011) A recent scenario of mass wasting and its impact on the transportation in Alborz Mountains, Iran using geo-information technology. Arab J Geosci 4:1337–1349. https://doi.org/10.1007/s12517-010-0238-7

Feizizadeh B, Blaschke T (2013) GIS-multicriteria decision analysis for landslide susceptibility mapping: comparing three methods for the Urmia lake basin. Iran Nat hazards 65:2105–2128. https://doi.org/10.1007/s11069-012-0463-3

Feizizadeh B, Abedi Gheshlaghi H, Bui DT (2020) An integrated approach of GIS and hybrid intelligence techniques applied for flood risk modeling. J Environ Plan Manag. https://doi.org/10.1080/09640568.2020.1775561

Feizizadeh B, Ronagh Z, Pourmoradian S et al (2021) An efficient GIS-based approach for sustainability assessment of urban drinking water consumption patterns: a study in Tabriz city. Iran Sustain Cities Soc 64:102584. https://doi.org/10.1016/j.scs.2020.102584

Ferrari R, Malcolm H, Neilson J et al (2018) Integrating distribution models and habitat classification maps into marine protected area planning. Estuar Coast Shelf Sci 212:40–50. https://doi.org/10.1016/j.ecss.2018.06.015

Gariano SL, Guzzetti F (2016) Landslides in a changing climate. Earth-Science Rev 162:227–252. https://doi.org/10.1016/j.earscirev.2016.08.011

Gorsevski PV, Jankowski P, Gessler PE (2006) An heuristic approach for mapping landslide hazard by integrating fuzzy logic with analytic hierarchy process. Control Cybern 35:121–146

Guan X, Liao S, Bai J et al (2017) Urban land-use classification by combining high-resolution optical and long-wave infrared images. Geo-spatial Inf Sci 20:299–308. https://doi.org/10.1080/10095020.2017.1403731

Hong T, Lee SH (2019) Integrating physics-based models with sensor data: an inverse modelling approach. Build Environ. https://doi.org/10.1016/j.buildenv.2019.03.006

Hong H, Pourghasemi HR, Pourtaghi ZS (2016) Landslide susceptibility assessment in Lianhua County (China): a comparison between a random forest data mining technique and bivariate and multivariate statistical models. Geomorphology 259:105–118. https://doi.org/10.1016/j.geomorph.2016.02.012

Hong H, Ilia I, Tsangaratos P et al (2017) A hybrid fuzzy weight of evidence method in landslide susceptibility analysis on the Wuyuan area, China. Geomorphology 290:1–16. https://doi.org/10.1016/j.geomorph.2017.04.002

Jaafari A, Najafi A, Pourghasemi HR et al (2014) GIS-based frequency ratio and index of entropy models for landslide susceptibility assessment in the Caspian forest, northern Iran. Int J Environ Sci Technol 11:909–926. https://doi.org/10.1007/s13762-013-0464-0

Jiménez-Perálvarez JD (2018) Landslide-risk mapping in a developing hilly area with limited information on landslide occurrence. Landslides 15:741–752. https://doi.org/10.1007/s10346-017-0903-y

Kalantar B, Pradhan B, Naghibi SA et al (2018) Assessment of the effects of training data selection on the landslide susceptibility mapping: a comparison between support vector machine (SVM), logistic regression (LR) and artificial neural networks (ANN). Geomat Nat Hazards Risk 9:49–69. https://doi.org/10.1080/19475705.2017.1407368

Kavzoglu T, Sahin EK, Colkesen I (2014) Landslide susceptibility mapping using GIS-based multi-criteria decision analysis, support vector machines, and logistic regression. Landslides 11:425–439. https://doi.org/10.1007/s10346-013-0391-7

Kavzoglu T, Sahin EK, Colkesen I (2015) Selecting optimal conditioning factors in shallow translational landslide susceptibility mapping using genetic algorithm. Eng Geol 192:101–112. https://doi.org/10.1016/j.enggeo.2015.04.004

Kornejady A, Pourghasemi HR (2019) Producing a spatially focused landslide susceptibility map using an ensemble of Shannon's entropy and fractal dimension (Case Study: Ziarat Watershed, Iran). In: Spatial modelling in GIS and R for earth and environmental sciences. Elsevier, pp 689–732. https://doi.org/10.1016/B978-0-12-815226-3.00032-6

Korup O, Görüm T, Hayakawa Y (2012) Without power? landslide inventories in the face of climate change. Earth Surf Process Landforms 37:92–99. https://doi.org/10.1002/esp.2248

Laamrani A, Valeria O, Bergeron Y et al (2015) Distinguishing and mapping permanent and reversible paludified landscapes in Canadian black spruce forests. Geoderma 237:88–97. https://doi.org/10.1016/j.geoderma.2014.08.011

Lee S, Min K (2001) Statistical analysis of landslide susceptibility at Yongin, Korea. Environ Geol 40:1095–1113. https://doi.org/10.1007/s002540100310

Luo W, Liu C-C (2018) Innovative landslide susceptibility mapping supported by geomorphon and geographical detector methods. Landslides 15:465–474. https://doi.org/10.1007/s10346-017-0893-9

McKean J, Roering J (2004) Objective landslide detection and surface morphology mapping using high-resolution airborne laser altimetry. Geomorphology 57:331–351. https://doi.org/10.1016/S0169-555X(03)00164-8

Melchiorre C, Matteucci M, Azzoni A, Zanchi A (2008) Artificial neural networks and cluster analysis in landslide susceptibility zonation. Geomorphology 94:379–400. https://doi.org/10.1016/j.geomorph.2006.10.035

Meng Q, Miao F, Zhen J et al (2016) GIS-based landslide susceptibility mapping with logistic regression, analytical hierarchy process, and combined fuzzy and support vector machine methods: a case study from Wolong Giant Panda Natural Reserve, China. Bull Eng Geol Environ 75:923–944. https://doi.org/10.1007/s10064-015-0786-x

Moayedi H, Mehrabi M, Mosallanezhad M et al (2019) Modification of landslide susceptibility mapping using optimized PSO-ANN technique. Eng Comput 35:967–984. https://doi.org/10.1007/s00366-018-0644-0

Nguyen VV, Pham BT, Vu BT et al (2019) Hybrid machine learning approaches for landslide susceptibility modeling. Forests 10:157. https://doi.org/10.3390/f10020157

Nhu V-H, Shirzadi A, Shahabi H et al (2020) Shallow landslide susceptibility mapping by random forest base classifier and its ensembles in a Semi-Arid region of Iran. Forests 11:421. https://doi.org/10.3390/f11040421

Nicu IC, Asăndulesei A (2018) GIS-based evaluation of diagnostic areas in landslide susceptibility analysis of Bahluieț River Basin (Moldavian Plateau, NE Romania). Are Neolithic sites in danger? Geomorphology 314:27–41. https://doi.org/10.1016/j.geomorph.2018.04.010

Ozdemir A (2020) A comparative study of the frequency ratio, analytical hierarchy process, artificial neural networks and fuzzy logic methods for landslide susceptibility mapping: Taşkent (Konya). Turkey Geotech Geol Eng. https://doi.org/10.1007/s10706-020-01284-8

Pham BT, Bui DT, Dholakia MB et al (2016) A comparative study of least square support vector machines and multiclass alternating decision trees for spatial prediction of rainfall-induced landslides in a tropical cyclones area. Geotech Geol Eng 34:1807–1824. https://doi.org/10.1007/s10706-016-9990-0

Pham BT, Prakash I, Bui DT (2018) Spatial prediction of landslides using a hybrid machine learning approach based on random subspace and classification and regression trees. Geomorphology 303:256–270. https://doi.org/10.1016/j.geomorph.2017.12.008

Pham BT, Jaafari A, Prakash I, Bui DT (2019) A novel hybrid intelligent model of support vector machines and the MultiBoost ensemble for landslide susceptibility modeling. Bull Eng Geol Environ 78:2865–2886. https://doi.org/10.1007/s10064-018-1281-y

Pham BT, Nguyen-Thoi T, Qi C et al (2020) Coupling RBF neural network with ensemble learning techniques for landslide susceptibility mapping. CATENA 195:104805. https://doi.org/10.1016/j.catena.2020.104805

Pourghasemi HR, Pradhan B, Gokceoglu C (2012) Application of fuzzy logic and analytical hierarchy process (AHP) to landslide susceptibility mapping at Haraz watershed. Iran Nat hazards 63:965–996. https://doi.org/10.1007/s11069-012-0217-2

Pourghasemi HR, Yansari ZT, Panagos P, Pradhan B (2018) Analysis and evaluation of landslide susceptibility: a review on articles published during 2005–2016 (periods of 2005–2012 and 2013–2016). Arab J Geosci 11:193. https://doi.org/10.1007/s12517-018-3531-5

Rahmati O, Moghaddam DD, Moosavi V et al (2019a) An automated python language-based tool for creating absence samples in groundwater potential mapping. Remote Sens 11:1375. https://doi.org/10.3390/rs11111375

Rahmati O, Yousefi S, Kalantari Z et al (2019b) Multi-hazard exposure mapping using machine learning techniques: A case study from Iran. Remote Sens 11:1943. https://doi.org/10.3390/rs11161943

Raja NB, Çiçek I, Türko\uglu N, et al (2017) Landslide susceptibility mapping of the Sera River Basin using logistic regression model. Nat Hazards 85:1323–1346. https://doi.org/10.1007/s11069-016-2591-7

Rajabi M, Valizadeh Kamran K, Abedi Gheshlaghi H (2016) Evaluation and zoning landslide hazard by using the analysis network process and artificial neural network (case study Azarshahr Chay basin). Quant Geomorphol Res 8:60–74

Reichenbach P, Rossi M, Malamud BD et al (2018) A review of statistically-based landslide susceptibility models. Earth-Science Rev 180:60–91. https://doi.org/10.1016/j.earscirev.2018.03.001

Rosi A, Tofani V, Tanteri L et al (2018) The new landslide inventory of Tuscany (Italy) updated with PS-InSAR: geomorphological features and landslide distribution. Landslides 15:5–19. https://doi.org/10.1007/s10346-017-0861-4

Sahana M, Sajjad H (2017) Evaluating effectiveness of frequency ratio, fuzzy logic and logistic regression models in assessing landslide susceptibility: a case from Rudraprayag district, India. J Mt Sci 14:2150–2167. https://doi.org/10.1007/s11629-017-4404-1

Samodra G, Chen G, Sartohadi J, Kasama K (2018) Generating landslide inventory by participatory mapping: an example in Purwosari Area, Yogyakarta, Java. Geomorphology 306:306–313. https://doi.org/10.1016/j.geomorph.2015.07.035

Sharma S, Mahajan AK (2019) A comparative assessment of information value, frequency ratio and analytical hierarchy process models for landslide susceptibility mapping of a Himalayan watershed, India. Bull Eng Geol Environ 78:2431–2448. https://doi.org/10.1007/s10064-018-1259-9

Sharma LP, Patel N, Ghose MK, Debnath P (2015) Development and application of Shannon's entropy integrated information value model for landslide susceptibility assessment and zonation in Sikkim Himalayas in India. Nat hazards 75:1555–1576. https://doi.org/10.1007/s11069-014-1378-y

Shirani K, Pasandi M, Arabameri A (2018) Landslide susceptibility assessment by Dempster-Shafer and index of entropy models, Sarkhoun basin, Southwestern Iran. Nat Hazards 93:1379–1418. https://doi.org/10.1007/s11069-018-3356-2

Shirzadi A, Bui DT, Pham BT et al (2017) Shallow landslide susceptibility assessment using a novel hybrid intelligence approach. Environ Earth Sci 76:60. https://doi.org/10.1007/s12665-016-6374-y

Swetha TV, Gopinath G (2020) Landslides susceptibility assessment by analytical network process: a case study for Kuttiyadi river basin (Western Ghats, southern India). SN Appl Sci 2:1–12. https://doi.org/10.1007/s42452-020-03574-5

Tehrany MS, Jones S, Shabani F (2019) Identifying the essential flood conditioning factors for flood prone area mapping using machine learning techniques. CATENA 175:174–192. https://doi.org/10.1016/j.catena.2018.12.011

Termeh SVR, Kornejady A, Pourghasemi HR, Keesstra S (2018) Flood susceptibility mapping using novel ensembles of adaptive neuro fuzzy inference system and metaheuristic algorithms. Sci Total Environ 615:438–451. https://doi.org/10.1016/j.scitotenv.2017.09.262

Tien Bui D, Pham BT, Nguyen QP, Hoang N-D (2016) Spatial prediction of rainfall-induced shallow landslides using hybrid integration approach of least-squares support vector machines and differential evolution optimization: a case study in Central Vietnam. Int J Digit Earth 9:1077–1097. https://doi.org/10.1080/17538947.2016.1169561

Tien Bui D, Shirzadi A, Shahabi H et al (2019) New ensemble models for shallow landslide susceptibility modelling in a semi-arid watershed. Forests 10:743. https://doi.org/10.3390/f10090743

Truong XL, Mitamura M, Kono Y et al (2018) Enhancing prediction performance of landslide susceptibility model using hybrid machine learning approach of bagging ensemble and logistic model tree. Appl Sci 8:1046. https://doi.org/10.3390/app8071046

Tsangaratos P, Loupasakis C, Nikolakopoulos K et al (2018) Developing a landslide susceptibility map based on remote sensing, fuzzy logic and expert knowledge of the Island of Lefkada. Greece Environ earth Sci 77:363. https://doi.org/10.1007/s12665-018-7548-6

Wagner PD, Fohrer N (2019) Gaining prediction accuracy in land use modelling by integrating modeled hydrologic variables. Environ Model Softw. https://doi.org/10.1016/j.envsoft.2019.02.011

Yalcin A, Reis S, Aydinoglu AC, Yomralioglu T (2011) A GIS-based comparative study of frequency ratio, analytical hierarchy process, bivariate statistics and logistics regression methods for landslide susceptibility mapping in Trabzon, NE Turkey. CATENA 85:274–287. https://doi.org/10.1016/j.catena.2011.01.014

Yang J, Song C, Yang Y et al (2019) New method for landslide susceptibility mapping supported by spatial logistic regression and geodetector: A case study of Duwen Highway Basin, Sichuan Province, China. Geomorphology 324:62–71. https://doi.org/10.1016/j.geomorph.2018.09.019

Yano A, Shinohara Y, Tsunetaka H et al (2019) Distribution of landslides caused by heavy rainfall events and an earthquake in northern Aso Volcano, Japan from 1955–2016. Geomorphology 327:533–541. https://doi.org/10.1016/j.geomorph.2018.11.024

Yilmaz I (2009) Landslide susceptibility mapping using frequency ratio, logistic regression, artificial neural networks and their comparison: a case study from Kat landslides (Tokat—Turkey). Comput Geosci 35:1125–1138. https://doi.org/10.1016/j.cageo.2008.08.007

Youssef AM (2015) Landslide susceptibility delineation in the Ar-Rayth area, Jizan, Kingdom of Saudi Arabia, using analytical hierarchy process, frequency ratio, and logistic regression models. Environ earth Sci 73:8499–8518. https://doi.org/10.1007/s12665-014-4008-9

Zêzere JL, Pereira S, Melo R et al (2017) Mapping landslide susceptibility using data-driven methods. Sci Total Environ 589:250–267. https://doi.org/10.1016/j.scitotenv.2017.02.188

Zhu A-X, Miao Y, Yang L et al (2018) Comparison of the presence-only method and presence-absence method in landslide susceptibility mapping. CATENA 171:222–233. https://doi.org/10.1016/j.catena.2018.07.012